RSC Advances

ROYAL SOCIETY OF CHEMISTRY

www.rsc.org/advances

Metal Nickel Nanoparticles In-Situ Generated in Rice Husk Char for Catalytic Reformation of Tar and Syngas from Biomass Pyrolytic Gasification

Yafei Shen [1]*, Chinnathan Areeprasert [1, 2], Bayu Prabowo [1], Fumitake Takahashi [1] and Kunio Yoshikawa [1]

[1] Department of Environmental Science and Technology, Interdisciplinary Graduate School of Science and Engineering, Tokyo Institute of Technology, G5-8, 4259 Nagatsuta, Midori-ku, Yokohama, 226-8502, Japan

[2] Department of Mechanical Engineering, Faculty of Engineering, Kasetsart University, 50 Ngam Wong Wan Rd, Ladyaow, Chatuchak, Bangkok, 10900, Thailand

ABSTRACT

This paper aims to propose a novel catalytic pyrolytic gasification technology for *in-situ* conversion of tar and syngas, accompanied by the silica-based nickel nanoparticles *in-situ* generated and highly dispersed in rice husk char (RHC), namely RHC Ni. Partial nickel oxides (i.e., NiO) in the carbon matrix of biochar can be carbothermally reduced into the metallic nickel (Ni^0) nanoparticles by reducing gases (e.g., CO) or carbon atoms during the biomass pyrolysis. Furthermore, due to the strong reducibility, the addition of sodium borohydride ($NaBH_4$) can significantly promote the generation of Ni^0 from the reduction of NiO, improving the biochar catalytic activity. The ultra-low tar yield can be achieved by pyrolysis of RH Ni and RH Ni-B at 750 ^oC, in terms of high tar conversion efficiencies of 96.9% and 98.6%, respectively, compared with the pyrolysis of raw RH. It is noteworthy that the condensable tar could be catalytically reformed into the small molecules of the non-condensable tar or gases, which contributes to improve the syngas fuel characteristics in favor of the power generation systems, corresponding to the lower heating value (LHV) of syngas increased from 10.25 to 11.32 MJ/m^3. Additionally, the increase of the polymolecularity Ni^0 was most likely caused by the disproportionated reaction and strong reducibility of $NaBH_4$. More importantly, the produced RHC Ni had good performances on catalytic conversion of tar (conversion efficiency, 96.5%) through co-pyrolysis with biomass. After deactivation, the waste RHC Ni might be easily regenerated via thermal treatment or directly catalytic gasified into the applicable syngas, accompanied by the production of the silica-based nickel nanoparticles.

Keywords: *biomass pyrolysis, tar conversion, rice husk char (RHC), nickel nanoparticles, amorphous silica*

***Corresponding Author**

Phone: +81-45-924-5507; fax: +81-45-924-5518

Email address: yafeisjtu@gmail.com; shen.y.ad@m.titech.ac.jp

1. INTRODUCTION

Owing to the rapid increase in the world's industrialization and population, the demand for energy is increasing; some new energy resources are needed to supplement the major conventional energy consumption, such as petroleum, coal and natural gas [1,2]. Biomass has been recognized as a renewable, inexpensive sustainable feedstock, environmental friendly and received considerable attention. Biomass is composed of cellulose, hemicelluloses and lignin, which can be transformed into fuels and valuable chemicals within a single facility. Furthermore, in the production of heat and power, the utilization of biomass derivatives mitigates the release of greenhouse gas (GHG) emissions through cycles of regrowth and combustion [3,4]. What's more, thermochemical conversion of degradation-resistant biomass wastes can not only resolve the problem of environmental contaminate, but also achieve the re-utilization of resources.

The application of thermochemical processes such as pyrolysis, gasification, combustion and liquefaction for energy recovery from biomass waste has attracted a growing attention by researchers [5]. Pyrolysis has attained much attention, as the process can be optimized to obtain liquid oils, product gases and biochars at the different temperature ranges. One of the major issues is to deal with biomass tar during the pyrolysis. Tar is a complex mixture of the condensable and non-condensable hydrocarbons including single ring to five-ring aromatic organic compounds with oxygen-containing hydrocarbons and polycyclic aromatic hydrocarbons (PAHs) [6,7]. Aromatic compounds present in tar, such as benzene and PAHs, are toxic and represent environmental hazards. Also, the condensable tar can deposit on the surfaces of filters, heat exchangers and engines, thereby reducing the component performance and increasing the maintenance requirements. Significantly, tar can polymerize to form more complex structures and aerosols, causing the catalysts deactivation. Tar removal technologies can be typically divided into two approaches [6]: gas cleaning treatment inside the gasifier (primary methods) and after the gasifier (secondary methods). Primary methods include the measures taken in the pyrolysis/gasification step to prevent tar formation in the furnaces or to transform it into the small molecular gases. Secondary methods include chemical or physical treatments in the downstream of the furnaces. Several approaches for tar elimination, such as physical treatment, thermal cracking, plasma-assisted cracking, and catalytic reforming, have been widely studied [7]. Among these measurements, the catalytic reforming process is most attractive technique for tar removal. The catalysts used in the reforming include metallic catalysts, mainly nickel based catalysts [8],

alkali metallic catalysts, dolomites, olivine [9] or a combination of metals on mineral substrate [10]. In addition, catalytic pyrolysis-reforming can significantly cut down the expenses of the follow-up tar elimination processes, such as physicochemical absorption (e.g., water, oil) and adsorption (e.g., activated carbon, biochar). Moreover, the classical gas cleaning technology based on scrubbing is not acceptable because of the poor efficiency on tar removal, wastewater production, and energy loss during gas cooling which reduces the overall process efficiency.

Catalytic treatment of pyrolysis vapors enables the cracking of organic molecules, leading to a decrease in liquid yield, and thereby to an increase in gas production. Regarding aromatic compounds, the main effect is deoxygenation of the compounds, but the aromatic rings are not destroyed and their concentration may even increase [11,12]. A dry mixing catalyst with biomass before pyrolysis produced similar results [13,14]. More pronounced effects on the yields of tar, char and gas have been obtained during the pyrolysis of metal-impregnated biomass [15-19]. Metal adsorption is mainly due to ion exchange with mineral cations naturally present in biomass: metal ions of the impregnation solution replace mineral cations that are released in solution [20]. Characterization of metal impregnated biomass revealed that impregnation enables uniform dispersion of the metal and intimate contact with the biomass [18,19]. As a consequence of the intimate contact, metal not only catalyzes volatile cracking, but also reactions in the lignocellulosic matrix, leading to significant changes in the yields of char and other products[16,21,22]. Bru et al.[15] obtained a significant tar reduction by nickel impregnation twice as much as iron impregnation. In addition, the catalytic effect increased the hydrogen production tripled with nickel.

With the increasing global concern over the rise in GHG emissions, there are great incentives for reducing the concentrations of both CO_2 and CH_4 in the atmosphere [23]. CO_2 produced along with syngas from biomass pyrolysis can also react catalytically with CH_4 at higher temperature [24]. Ni-based catalysts are cost-effective and active for dry reforming of tar and methane, but also more prone to carbon formation than noble metals [25-28]. Courson et al.[29] proved that the NiO_2/olivine[$(Mg,Fe)_2SiO_4$] exhibited a high activity in dry-reforming (95% methane conversion) and steam-reforming (88% methane conversion) and yield in syngas (80% and 75% CO yield, respectively) in biomass gasification. Xu et al. [30,31] studied the influence of boron addition on the activity and the stability of Ni catalysts for steam reforming of methane. It showed a positive effect of small amounts of boron (0.5 and 1 wt%) on enhancing the stability of

Ni/Al_2O_3 catalyst in methane steam reforming, and limit coking, without compromising the activity[31]. Although the activity of boron-modified catalysts also declines with time-on-stream, less carbon could be formed compared to the unpromoted one. Regarding to dry reforming of methane, boron was used so far with another approach as support component or modifier to control the surface acidity and nickel dispersion [23,32]. Besides, adding boron in such a low concentration range is known to reduce sulfur deactivation [33,34]. Up to now, the boron-modified nickel catalysts for tar conversion during biomass pyrolysis have been rarely studied. In the present work, a novel *in-situ* catalytic conversion of tar and vapor derived from the pyrolysis process of biomass, which is pretreated by nickel impregnation, and modified by sodium borohydride ($NaBH_4$). Subsequently, the metallic nickel (Ni^0) nanoparticles can be *in-situ* generated in the rice husk char (RHC), namely RHC Ni, which was preliminary investigated for catalytic conversion of tar via the co-pyrolysis with biomass.

2. MATERIALS AND METHODS

2.1. Characterization of Biomass Samples

The biomass feedstock of rice husk (RH) was collected from Thailand. Table 1 shows the proximate and ultimate analysis of RHs and RH ash (RHA), which were conducted by the elemental analyzer (*Vario Micro Cube, Elementar, Germany*) and the DTG-50 (*Shimazu, Nakagyo-ku, Kyoto, Japan*), respectively. The elemental contents of nickel (Ni) and boron (B) were determined by the inductively coupled plasma mass spectrometry (ICP-MS, *ELAN DRC-e, PerkinElmer, USA*). The metal cations adsorption capacity of char relies on the preparation methods and conditions, such as char surface characteristics (e.g., specific surface area, pore size), impregnation temperature, metal cation type. Thereby, it was assumed that most of nickel cations can be smoothly adsorbed by RHC, so the nickel content in the RHC Ni was less than 60 mg/g. In addition, the chemical composition of the RHA was analyzed by the X-ray fluorescence (XRF, *Shimazu, Rayny EDX 700, Japan*). From the chemical composition of RHA, it can be indicated that RH is very abrasive and wears conveying elements very quickly ascribe to the high silica contents.

Table 1. Properties of RH, RHC and RHA

	Ultimate analysis (wt.%, dry & ash free basis)					Proximate analysis (wt.%, dry basis/as received)				S_{BET} (m^2/g)
	C	*H*	*O* [*]	*N*	*S*	*VM* [c]	*FC* [d]	*Ash*	*Moisture*	
RH	37.9	6.3	55.3	0.4	0.1	60.5/ 59.3	11.9/ 10.4	22.0/ 20.5	5.6/ 9.8	2.2
RHC	64.8	2.4	35.1	0.1	0	11.7	34.3	52.0	2.0	117.0 [b]
RHA	9.5	0.3	90.2	0	0	5.4	7.8	85.3	1.5	65.4
Chemical composition of RHA (wt.%)										
SiO_2	Al_2O_3	Fe_2O_3	CaO	MgO	Na_2O	K_2O	Zn (ppm)	Mn (ppm)	Cu (ppm)	Cd (ppm)
94.64	0.06	0.23	1.88	0.96	0.39	0.58	18.20	52.24	32.17	0.48

[a] *Calculated by mass difference;* [b] *700 °C char, changed with pyrolysis method;*
[c] *VM-volatile matters;* [d] *FC-fixed carbon.*

The raw RH was impregnated with aqueous nickel nitrate solutions [$Ni(NO_3)_2 \cdot 6H_2O$, *Wako Pure Chemical Industries, Ltd., Japan*] as the mimetic nickel precursor. It could be inferred that the increase in nitrogen (N) content of RHs was attributed to the adsorption of $Ni(NO_3)^+$ and ammonium NH_4^+ cations present in the solution, along with the possible adsorption of NO_3^- anions. Besides, the hydrogen (H) content in the nickel cations (Ni^{2+}) impregnated RH was decreased due to the deprotonation of the oxygenated surface groups necessary for adsorption of the Ni^{2+} species [19], while the slight increase of hydrogen (H) content was attributed to the hydrogenation by the strong reducibility of BH_4^- or activated hydrogen (H*) from $NaBH_4$ hydrolysis. Fig.1 shows the incipient wetness impregnation of nickel cations along with $NaBH_4$ modification for RH. It could be observed that $NaBH_4$ was hydrolyzed rapidly, when it was added into the Ni^{2+} solution (Fig.1B). A large amount of gas bubbles produced tempestuously might contribute to improve the pores dimension (i.e., macropores, mesopores, and micropores) and distribution, accordingly enhancing the RH adsorption performance for metal cations based on the major reactions (R1-R9). After impregnation and drying overnight at 105 °C, the pretreated dry-basis RH samples (i.e., RH, RH Ni and RH Ni-B) were dry-stored for further use. In addition, the organic functional groups of RH samples were investigated by the fourier transform infrared spectroscopy (*FT-IR, JIR-SPX200, JEOL, Japan*) before and after pyrolysis. Subsequently, the residual biochars derived from RHs pyrolysis were characterized by the X-ray diffraction (*XRD, D8 Discover, Bruker AXS, Germany*) and the transmission electron

microscopy-energy dispersive spectroscopy (*TEM-EDS, JEM-2010F, JEOL, Japan*), respectively.

$$5Ni(NO_3)_2 + 24H_2O \rightarrow Ni^{2+} + 4[Ni(H_2O)_6]^{2+} + 10NO_3^- \quad (R1)$$

$$[Ni(H_2O)_6]^{2+} \rightarrow Ni(OH)_2 + 2H_3O^+ + 2H_2O \ (thermal\ decomposition) \quad (R2)$$

$$Ni(OH)_2 \rightarrow NiO + H_2O \quad (R3)$$

$$BH_4^- + x\ Ni^{2+} \rightarrow Ni_xB\ (x = 1\text{-}3) + 2H_2\uparrow \quad (R4)$$

$$BH_4^- + 2Ni^{2+} \rightarrow Ni_2B\downarrow\ (black\ precipitate) + 2H_2\uparrow \quad (R5)$$

$$BH_4^- + 2H_2O \rightarrow BO_2^- + 4H_2\uparrow\ (Ni_2B\ catalytic\ hydrolysis) \quad (R6)$$

$$Ni^{2+} + 2BO_2^- \rightarrow Ni(BO_2)_2 \quad (R7)$$

$$3Ni(BO_2)_2 + 2Ni_2B \rightarrow 7Ni^0\ (polymolecularity) + 4B_2O_3 \quad (R8)$$

$$Ni^{2+} + H_2 \rightarrow Ni^0 + 2H^+\ (Ni_2B\ catalytic\ hydrogenation) \quad (R9)$$

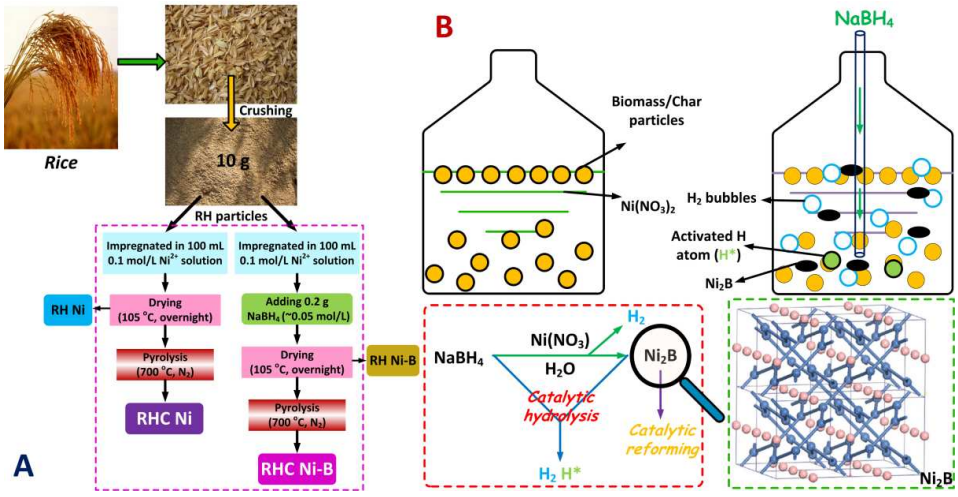

Figure 1. Schematic diagrams of (A) RH impregnated with $Ni(NO_3)_2$ and (B) modified by $NaBH_4$

2.2. Biomass Pyrolysis-Reforming System

The experimental setup includes a gas supplying system, an online syngas analysis system, a gas cleaning system and a two-stage pyrolysis-reforming reactor, which was made from quartz and divided into three parts, an outer tube, an inner tube, and a top cover with a feeding port and a gas inlet. A sintered quartz porous plate was fixed in each tube, which was surrounded by a two-zone electric furnace. RH feedstock was prepared by crushing and sieving with the particle size below 5.0 mm. Initially, both the pyrolyzer (*first zone*) and the reformer (*second zone*) temperatures were heated up to 750 °C. Then, the inert carrier gas (i.e., N_2) with a flow rate of 1.0 L/min was continuously injected into the pyrolyzer to blow away the

residual gases in the entire system. When the prepared biomass sample (i.e., RHs, 10 g) was fed into the pyrolyzer, the volatile matters of it could be rapidly released in the forms of syngas and tar. By means of the heat in the first zone, biomass tar can be *in-situ* cracked and transformed into the small molecules by a series of thermal catalytic reactions. The residual tar was condensed and collected in the gas cleaning unit.

2.3. Sampling and Analysis

The gravimetric tar called heavy tar can be condensed, sampled and determined by weighing [35]. And the chemical composition of the tar samples were determined by the gas chromatography-mass spectrometer (*GC-MS*, *Shimazu, GCMS-QP2010*). Meanwhile, the produced gases, mainly in the forms H_2, CH_4, CO, CO_2, and C2 hydrocarbons (i.e., C_2H_4, C_2H_6) were collected using an air bag for gas collection at the outlet and measured by a micro gas chromatography (*Agilent, Micro GC, 3000A*) fitted with a thermal conductivity detector (TCD). Each trial was maintained for 10 min to ensure a good material balance. And repeatability experiments were performed on the reactor system to ensure the reliability and suitability of the system. Thus, the collected tar sample was the total quantity of tars generated from these repeatability experiments.

3. RESULTS AND DISCUSSIONS

3.1. Pyrolysis Products from RHs

The pyrolysis product yields of the RHs were shown in Table 2. The increase yield of solid residues (i.e., char) could be ascribed to the decrease of volatiles and the increase of nickel cation. In addition, the high conversion efficiencies of the condensable tar can be obtained by 96.9% (RH Ni) and 98.6% (RH Ni-B) via nickel impregnation and $NaBH_4$ modification (Figure S-1), respectively. It also can be observed the condensable tar was significantly reduced according to the color appearances of the condensates. It is noteworthy that the condensable tar is transformed into the non-condensable tar, thereby improving the fuel characteristics (e.g., heating value) of product gas in favor of the power generation systems. However, compared to the raw RH and RH Ni-B, the RH Ni can produce more syngas after pyrolysis. It is most likely that, on one hand, the removed tar was converted into the extra gases by thermochemical reactions (i.e., cracking, reforming) with the nickel catalysis effect; on the other hand, the nickel catalyst could enhance the pyrolysis efficiency and restrain at source the formation of macromolecular tar due to polymerization. Furthermore, the syngas properties got improved by nickel impregnation and $NaBH_4$

modification. For instance, H_2 concentration increased from 17.3% to 47.6%, accordingly the volume concentration ratio of H_2 and CO (H_2/CO) increased from 0.44 to 1.28. And the decrease of CH_4 and CO_2 may be attributed to a series of heterogeneous and homogeneous chemical reactions (R10-R22) via nickel catalysis at high temperatures [23,32]. Without injecting the steam, the water gas shift (WGS) reaction (R16) was not effective, so the H_2/CO was still low, unsuitable to be directly employed for chemical synthesis, e.g., *Fischer-Tropsch* (F-T) synthesis (H_2/CO ≥ 2). In addition, the lower heating value (LHV) of produced syngas calculated by the empirical formula was increased from 10.25 to 11.32 MJ/m^3. From the results in Table 2, it can conclude that the nickel impregnation and $NaBH_4$ modification is an effective pretreatment approach to realize tar *in-situ* catalytic conversion during biomass pyrolytic gasification. Besides, the use of biomass derived materials has been widely employed for heavy metals removal from aqueous solutions. Indeed, the numerous oxygenated functional groups (carboxyl, carbonyl, hydroxyl and ether) present in the biomacromolecules can be used as ligands for metal complexation in aqueous media, so a high metal dispersion into biomass matrix is obtained by the property of biomass constituting macromolecules, mainly including cellulose, hemicellulose and lignin. Because of the metal complexation property, wide availability and low-cost, natural polysaccharides are being given considerable attention for supported catalyst preparation [18]. Here, this catalytic pyrolysis technology would be a potential approach for *in-situ* preparation of nickel nanoparticles encapsulated in amorphous carbon matrix as described below. In these cases, an integrated concept of heavy metal treatment with biomass catalytic pyrolysis can be proposed in Scheme 2. Heavy metal wastewater (e.g., nickel electroplating wastewater) is preliminary concentrated and treated by biomass/biochar (e.g., RH, RHC) adsorption under the atmospheric or vaccum pressure. Generally, the vacuum impregnation technique could promote the formation of inner-sphere surface complexes, while impregnation in the atmospheric pressure seems to promote electrostatic interactions with the outer hydration sphere of nickel cation Ni^{2+} (outer-sphere complex), or the formation of hydrogen bonds [19]. Then, the adsorption saturated biomass is naturally dried and pyrolyzed at high temperature in the absence of oxygen. Finally, both the syngas with low-tar content and the metal nanoparticle catalysts (e.g., nano Ni/SiO_2 from RH Ni) are obtained. In addition, the metal nickel (Ni^0) nanoparticles embedded in RHC can be recycled and used for tar reformation or other applications.

$$\text{Biomass} \rightarrow CO + H_2 + CO_2 + CH_4 + H_2O + C_nH_m + \text{Tar}_{(CxHy,\ CxHyOz)} + \text{Char} \quad \text{(R10)}$$

$$C_nH_m \rightarrow nCO + (m/2)H_2 \quad \text{(R11)}$$

$$C_nH_m + nH_2O \rightarrow nCO + (m+2n)/2H_2 \quad \text{(R12)}$$

225 $C_nH_m + nCO_2 \rightarrow 2nCO + m/2H_2$ (R13)

226 $C_nH_m \rightarrow nCO + (m/2)\ H_2$ (R14)

227 $CH_4 + 0.5O_2 \rightarrow CO + 2H_2$ $\Delta H = -36$ kJ/mol (R15)

228 $CO + H_2O \rightarrow CO_2 + H_2$ $\Delta H = -41$ kJ/mol (R16)

229 $CH_4 \rightarrow C + 2H_2$ $\Delta H = +75$ kJ/mol (R17)

230 $C_nH_m \rightarrow nC + (m/2)H_2$ $(2 \le n \le 4)$ (R18)

231 $C + H_2O \rightarrow CO + H_2$ $\Delta H = +131$ kJ/mol (R19)

232 $C + CO_2 \rightarrow 2CO$ $\Delta H = +172$ kJ/mol (R20)

233 $CH_4 + H_2O \rightarrow CO + 3H_2$ $\Delta H = +206$ kJ/mol (R21)

234 $CH_4 + CO_2 \rightarrow 2CO + 2H_2$ $\Delta H = +247$ kJ/mol (R22)

235

236 **Table 2. The Products Derived from RH, RH Ni and RH Ni-B Pyrolysis at 750 °C**

	RH	RH Ni	RH Ni-B
Pyrolysis Products Yields (mg/g)			
Char	325.3	368.3	392.0
Tar [a]	86.5	2.7	1.2
Gas [b]	588.2	629.0	606.8
Syngas Composition (vol.%)			
CO	39.5	34.2	37.1
H_2	17.3	38.6	47.6
CH_4	9.5	6.4	4.2
CO_2	25.0	18.4	10.3
≥C2 [c]	8.7	2.4	0.8
H_2/CO	0.44	1.13	1.28
LHV (MJ/m^3) [d]	10.25	10.77	11.32

[a] The gravimetric tar (condensable tar) derived from RH pyrolysis at 750 °C; [b] The product gas estimated by difference include light tar (non-condensable tar) and other impurities; [c] By difference;

[d] $\mathrm{LHV}(kJ/m^3) = [30(CO) + 25.7(H_2) + 85.4(CH_4)] \times 4.2$

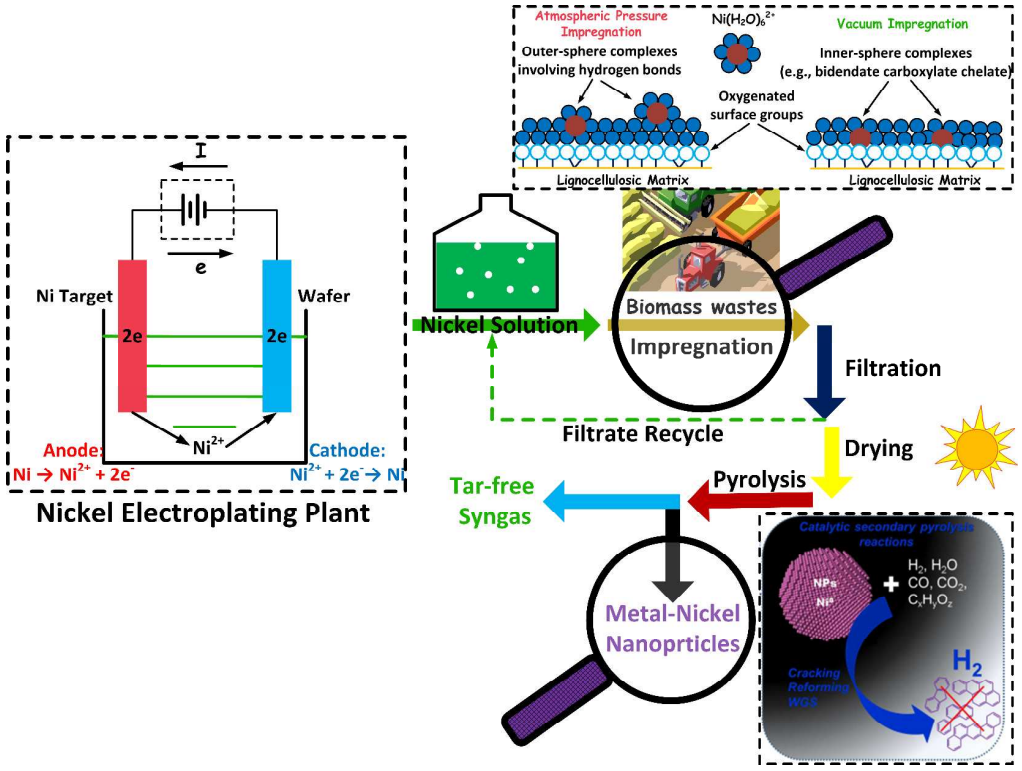

Scheme 2. An integrated concept of heavy metal treatment with biomass wastes catalytic pyrolysis

3.2. Thermogravimetric (TG) Analysis of RHs

TG analysis of three RH samples (~10 mg) was investigated at a 20 °C/min heating rate to an ultimate temperature of 800 °C with a holding time of 10 min under the nitrogen (N_2) condition. With the rise in temperature, weight loss of the sample was continuously recorded. This raw data was used to calculate TG and differential TG (DTG) curves, shown in Fig.2A. Obviously, the main weight loss occurs between 250 and 550 °C due to the devolatilization, especially in terms of mass loss around 300 °C corresponding to the cellulose/hemicellulose/lignin degradation, while the mass loss in the temperature ranges of 350-550 °C corresponds to the biochar decomposition [36]. Compared to the RH Ni and RH Ni-B, the raw RH initially tended to decompose at a lower temperature and a lower rate, most likely producing more condensable tar. When the heating temperature increased to 500 °C or above, the pyrolysis efficiency of RH can be improved by adding small amounts of $NaBH_4$. From DTG curves, it is clearly observed that the maximal devolatilization rate could be decreased by nickel cations impregnation. However, $NaBH_4$ modification can improve the maximal devolatilization rate compared to the onefold Ni used. Fig.2B shows the TG and DTG curves of the solid RHC samples (i.e., RHC, RHC Ni and RHC Ni-B) derived from RHs pyrolysis at

750 °C. When the heating temperature was below 400 °C, the RHC can keep much stable. The higher moisture content of RHC indicated that it can easily adsorb water from the surroundings because of its hydrophily. Thus, it may also conclude that the temperature range of 400-500 °C could be selected for thermal regeneration of the RHC Ni catalysts using the waste heat in the pyrolyzer. After that, the weights of them were slightly reduced in a constant rate. The RH Ni and RH Ni-B showed a similar decomposition rate corresponding to the first-order kinetics, which is higher than the decomposition rate of raw RH in the range of 600-800 °C (Fig.2C). It may be attributed to the decomposition of residual volatiles and the carbon reaction of char (e.g., *Boudouard reaction*). When the heating temperature was increased up to 800 °C, the weight of RHC can keep constant. The lower mass loss ratio of RHC Ni-B can be attributed to the high-efficiency devolatilization in the initial pyrolysis stage, so the devolatilization rate can be enhanced by the nickel impregnation. Thus, it is inferred that the addition of sodium borohydride might modify the chemical structures of organic functional groups in biomass, then improving the pyrolytic gasification efficiency.

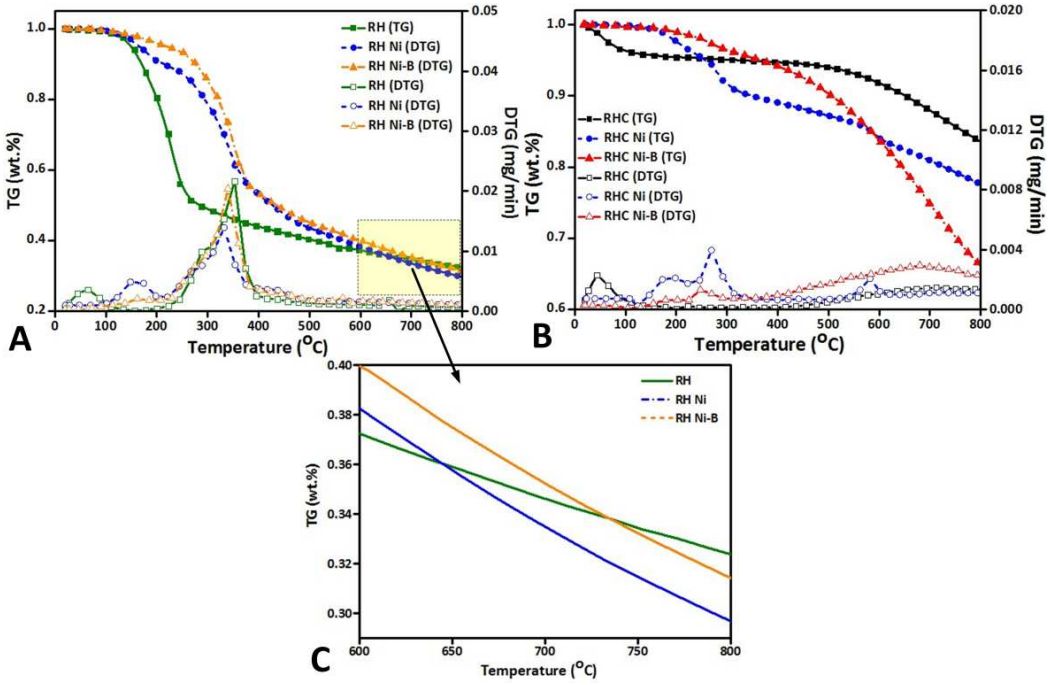

Figure 2. TG and DTG curves of (A) RHs and (B) RHCs under the nitrogen condition

3.3. FTIR Analysis of RHs

The FTIR spectra of three RHs were shown in Fig.3. It is known the typical components of biomass are cellulose, hemicellulose and lignin, so their typical functional groups and the IR signal with the possible

compounds are similar [37,38]. It can be observed that three RH samples are most likely consisted of acid, methanol, alkyl, aliphatics, aromatics and ketone with different oxygenated functional groups, e.g., O-H (3500-3200 cm^{-1}), -C=O (1735-1727 cm^{-1}, 1670-1630 cm^{-1}), COO^- groups in carboxylate (1400-1310 cm^{-1}), C-O-C (1250-1270 cm^{-1}, 1170 cm^{-1}), and C-O-(H) (1050 cm^{-1}), etc. The oxygen-free organic functional groups (e.g., hydrocarbons), such as $-CH_3/-CH_2-$ (2990-2850 cm^{-1}), O=C=O (2410-2280 cm^{-1}), benzene rings in aromatic organic compounds (1515-1485 cm^{-1}), benzene derivatives (890-805 cm^{-1}, 580-420 cm^{-1}) can also be detected in the RHs (Fig.3A). After pre-treated by Ni and Ni-B, the absorption peaks assigned to some organic functional groups in RH changed too much, such as COO^- groups in carboxylic acid salts (1400-1310 cm^{-1}, symmetrical strech), Si-O-Si (1100-1000 cm^{-1}, anti-symmetrical strech), while majority of the organic functional groups had small changes (Fig.3B), indicating that the pretreatment mildly destroyed the chemical structures of macromolecular organic functional groups in RHs. Significantly, the absorption peaks of several organic functional groups in RH, e.g., C-N-C in amines (407 cm^{-1}), rings in benzene derivatives (580, 569, 558 and 520 cm^{-1}), disappeared after pretreatment by $NaBH_4$. In addition, the disappeared peaks of the sulfur-containing functional groups in RH, such as C-S (600 cm^{-1}, strech) (Fig.3C), most likely were caused by the reductive sulfur removal due to the strong reducibility of $NaBH_4$ [39]. It implies that $NaBH_4$ modification is quite suitable to pretreat the high-sulfur fuels like coals, inhibiting the catalysts sulfur deactivation [33]. However, the IR absorption peak of C-OH in alcohol (669 cm^{-1}, bending) was enhanced probably due to the partial hydrolysis of lignin, etc. Organic functional groups in RHs mainly distribute in the range of 2000-400 cm^{-1}. In particular, Fig.3D reveals some remarkable changes in the range of 1800 and 1200 cm^{-1}. These spectra modifications mainly concerned the C=O and C-O bonds associated with the carboxyl function of the 4-O-methy-glucuronic the acid units of xylan (decreased intensities of the streching bands for C=O bond in aldehydes at ~1735 cm^{-1} and -OH bond in carboxylic acids at ~1423 cm^{-1}, and increased intensities of the symmetrical(υ_s) and anti-symmetrical(υ_{as}) streching bands for $(O-C=O)^-$ bond of the carboxylic acid salts at ~1385 and 1342 cm^{-1}). The streching bands for $(O-C=O)^-$ bond of the carboxylate seemed to increase proportionally with the Ni content of the sample, which effectively confirmed that these bands were associated with the presence of nickel in the RH. In addition, the $\Delta\upsilon$ between the two streching modes υ_s and υ_{as} (< 43 cm^{-1}) suggested intense coordination of the bidentate chelate type between the nickel and the carboxylate group[19]. Therefore, it clearly showed that the carboxylic acid functions of the hemicelluloses can play the role of ligands in forming the coordination complexes with the Ni^{2+} cation.

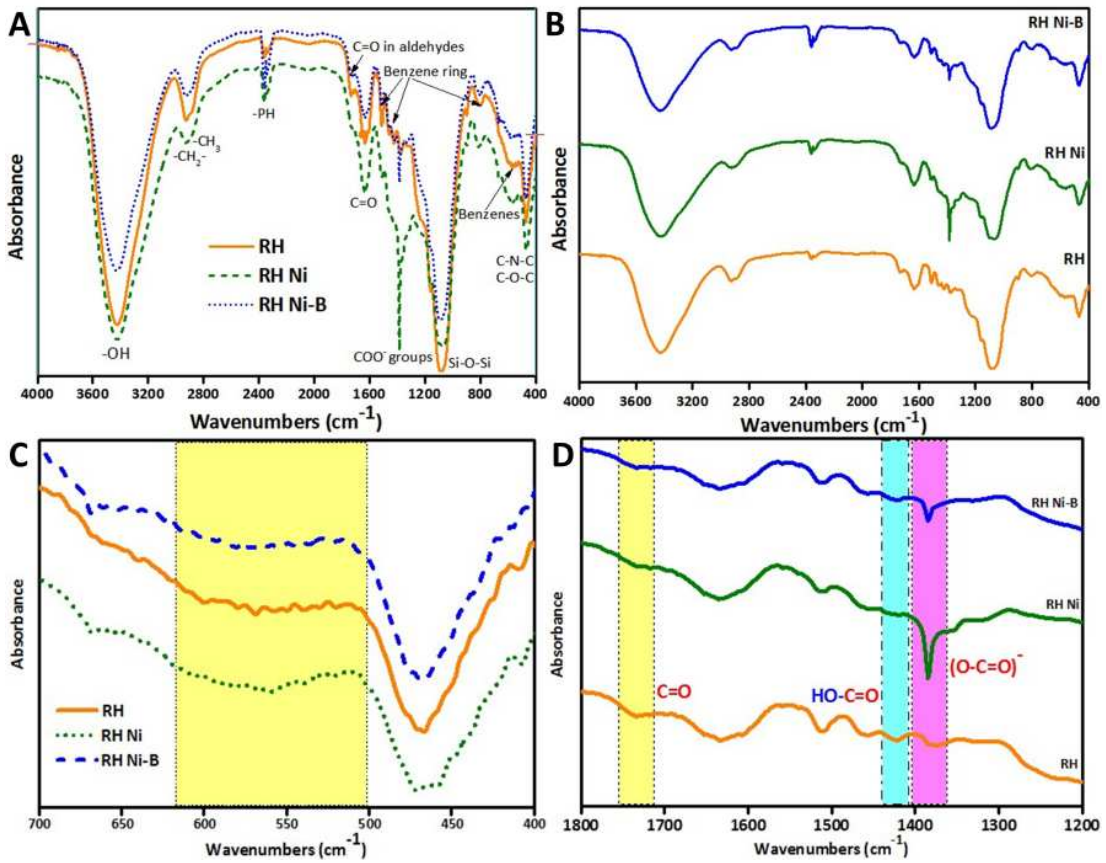

Figure 3. FTIR spectra of RH, RH Ni and RH Ni-B

Besides, the biomass pretreatment via nickel impregnation and $NaBH_4$ modification has other merits, such as ion exchange, deoxygenation, hydrogenolysis and carbon chains formation. As shown in Scheme 2, the IR adsorption peaks of $-(CH_2)_n-$ in hydrocarbons bands between 740-720 cm^{-1} appeared in the addition of $NaBH_4$. It indicated that $NaBH_4$ modification can tenderly break the carbon structures of macromolecular organic hydrocarbon compounds (e.g., cellulose, hemicellulose, lignin) into the $-(CH_2)_n-$ rocking in the long chains under the hot alkaline condition [40]. Nevertheless, the hydrolysis is not thoroughly without enzymatic saccharification [41]. Thus, the possible mechanism of long hydrocarbon chains formation by $NaBH_4$ modification can be deduced and proposed as follows (Scheme 2). These long chains were unstable and easily decomposed via thermochemical reactions contributing to the slight improvement of devolatilization efficiency. It should be noted that the polymolecularity Ni^0 can be generated due to the disproportionated reaction and the strong reducing property of $NaBH_4$ (R6 and R7).

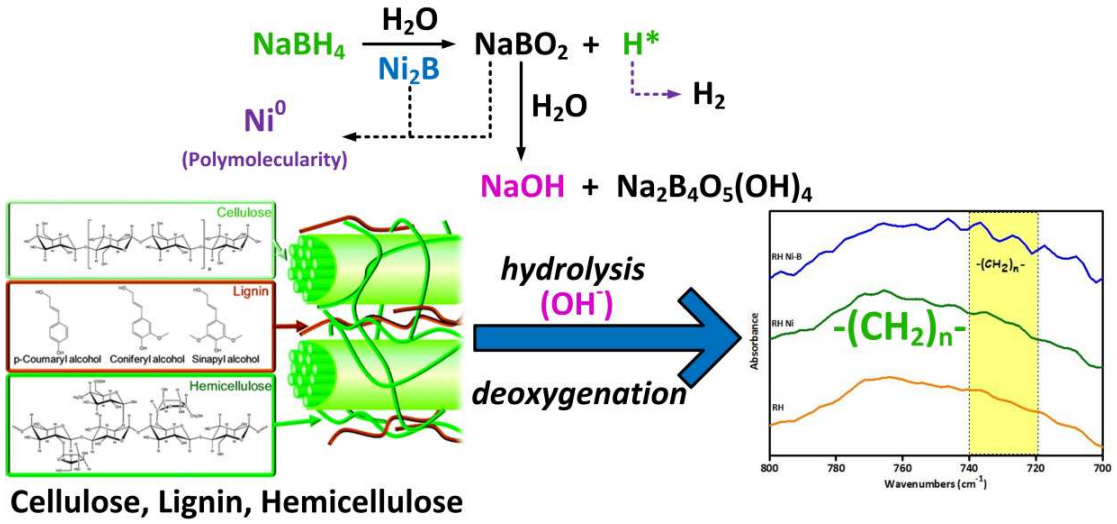

Scheme 2. Possible mechanism of long hydrocarbon chains formation by $NaBH_4$ modification

3.4. GC-MS Analysis of Tar

Figure S-2 shows the GC-MS analytical spectra of the collected tar samples from RH, RH Ni and RH Ni-B pyrolysis at 700 °C. In the GC spectrum, nearly 30 peaks were observed. MS spectra of these peaks were identified using the MS database and listed in Table 3. The most important and abundant organic compounds are styrene, phenol and naphthalene, which were identified as the main tar compounds derived from pyrolysis of wood samples. Lu et al. [43] also found that benzene derivatives, phenol derivatives, alkanes, cycloalkanes and aromatic hydrocarbons were the main compounds in the bio-oils from RH fast pyrolysis at lower temperature. In this research, the organic compounds in the condensed tar from RH pyrolysis at 750 °C existed mainly in the forms of light tar compounds (i.e., benzene, naphthalene) and oxygenated aromatic compounds (i.e., phenols). Additionally, only small amounts of the PAHs, e.g., phenanthrene, which was known to be carcinogenic or mutagenic, had been detected. It could be attributed to the higher pyrolysis and reforming temperature without causing the polymerization reactions. It is noteworthy that with nickel impregnation, the absorption peak intensities of tar compounds from RH pyrolysis were significantly decreased or disappeared. In Table 3, it can be seen that after pyrolysis of RH Ni and RH Ni-B, the polycyclic aromatics (e.g., phenanthrene) were significantly reduced in the residual tar compounds, mainly consisting of naphthalene and phenol derivates (e.g., 2-Ethyl-phenol). It can indicate that these aromatic tar compounds were more difficult to be transformed compared with the single-ring tar compounds, such as phenol, indene, and benzene. Thus, this catalytic pyrolysis technology

can remarkably inhibit the polymerization of small molecular tars (e.g., nascent tars) at source, thereby reducing the follow-up macromolecular tar formation and condensation. Scheme 3 is the representative molecular species showing tars evolution during biomass catalytic pyrolytic gasification. At lower temperatures, the primary pyrolytic products of the biomass individual components (e.g., lignin, cellulose and hemicellulose) are formed, which have a significant amount of oxygen and many have high molecular weights. As the temperature is increased, these products are cracked into the small pieces of molecular organic compounds (e.g., benzene derivatives). These cracking reactions also result in the formation of the useful syngas components (e.g., CO and H_2). Eventually, small hydrocarbon molecules and radicals could recombine as usual to form PAHs through the mechanisms that have been demonstrated in hydrocarbon combustion chemistry; PAHs are prevalent in tars that are observed during biomass pyrolysis/gasification [44]. Herein, the smaller hydrocarbon molecules and radicals might be cracked and transformed at sources to the extra syngas, restraining the formation of macromolecular organics due to polymerization.

Table 3. Main Identified Organic Compounds in the Collected Tar from RHs Pyrolysis at 750 °C

Residence Time (min)	Main Identified Compounds	Molecular Formula	Concentration (%)		
			RH	RH Ni	RH Ni-B
3.483	5-(2-Amino-2-carboxyethyl)-2-hydroxybenzoic acid	$C_{10}H_{11}NO_5$	4.77	3.14	5.41
4.375	Pyridine	$C_{10}H_8$	5.13	-	-
4.8	Benzene	C_6H_6	7.69	2.33	2.3
6.958	Naphthalene	$C_{10}H_8$	37.37	26.11	9.61
8.05	Phenol	C_6H_6O	5.45	-	-
8.758	3-Methyl-1,2-cyclopentanedione	$C_6H_8O_2$	7.72	26.59	12.16
9.342	Indene	C_9H_8	5.93	-	-
9.8	Methyl-phenol	C_7H_8O	1.9	-	1.53
10.283	Acenaphthalene	$C_{12}H_8$	3.07	-	-
10.717	Biphenylene	$C_{12}H_8$	3.34	-	-
10.808	2-Methyl-benzofuran	C_9H_8O	1.98	-	-
11.008	2-Ethyl-phenol	$C_8H_{10}O$	2.39	16.76	17.41
12.217	Methyl triacetic lactone	$C_7H_8O_3$	0.64	-	-
12.967	2,3,6-Trimethyl-phenol	$C_9H_{12}O$	1.91	-	-

13.025	4-Ethyl-2-methyl-phenol	$C_9H_{12}O$	1.62	7.84	8.02
14.508	3-Methyl-1,2-benzenediol	$C_7H_8O_2$	2.4	-	-
14.833	Indenol	C_9H_8O	5.45	3.18	2.48
17.208	Naphthalenol	$C_{10}H_8O$	2.15	2.24	1.8
19.7	Fluoranthene	$C_{16}H_{10}$	5.64	-	-
20.45	Trimethylsilyl 2,6-bis[(trimethylsilyl)oxy]benzoate	$C_{16}H_{30}O_4Si_3$	2.42	1.52	1.19
22.758	Phenanthrene	$C_{14}H_{10}$	3.32	1.32	-
24.3	3-Methylhenicosane	$C_{22}H_{46}$	1.77	-	-
24.475	Octadeamethyl-cyclononasiloxane	$C_{18}H_{54}O_9Si_9$	1.98	1.46	1.02
25.892	Benzoic acid, 2,6-bis[(trimethylsilyl)oxy]-, trimethylsilyl ester	$C_{16}H_{30}O_4Si_3$	1.91	0.93	3.12
26.65	Tetradecane	$C_{14}H_{30}$	4.8	-	-
27.108	N-Cholestan-4-ylacetamide	$C_{29}H_{51}NO$	2.4	0.86	-
28.367	Trimethylsilyl 2,6-bis[(trimethylsilyl)oxy]benzoate	$C_{16}H_{30}O_4Si_3$	2.46	-	-
29.958	Benzenamine	$C_{28}H_{43}N$	2.33	0.88	-

Note: - means undetected

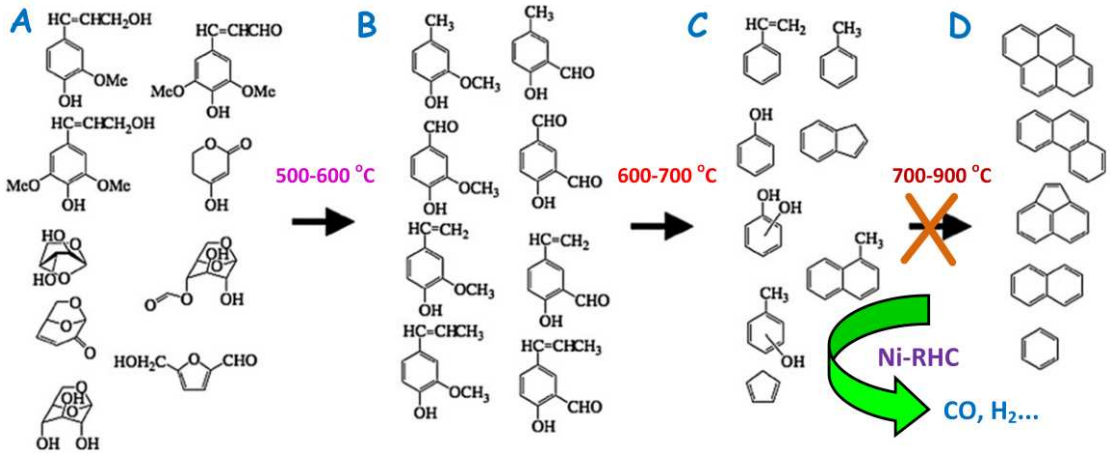

Scheme 3. Representative molecular species showing tars evolution during catalytic pyrolysis of biomass. (A) Primary pyrolysis products are formed at low temperatures (500-600 °C); (B and C) These products can be cracked or catalytic reformed at intermediate temperatures (600-700 °C); (D) PAHs are formed at higher temperatures (700-900 °C).

3.5. FTIR Analysis of RHC

The peak intensities of organic functional groups in RH were greatly changed after pyrolysis (Figure S-3A). Obviously, the absorption peak of -CH_3/-CH_2- in aliphatic compounds at 2896 cm^{-1} disappeared due to thermal cracking. In addition, the intensities of the streching band for -OH bond in alcohols and phenols at ~3424 cm^{-1}, the streching bands for C=O bond between 1735 and 1630 cm^{-1}, and the streching bands for the $(O\text{-}C{=}O)^-$ bond of the carboxylate at ~1385 cm^{-1}, and the streching band of the C-O-H in secondary and tertiary alcohols at ~1080 cm^{-1} showed a significant decrease after pyrolysis. It suggested that oxygen-containing functional groups, such as alcohols, phenols, can be easily cracked and deoxygenated by a series of thermochemical reactions. In general, the peak intensity of the naphthalenes bands at 490-465 cm^{-1} decreased after pyrolysis, while it presented a slight increase in the nickel impregnated RHs (i.e., RH Ni, RH Ni-B). It is possible that the primary tars (e.g., acetol, acetic acid and guaiacols) and secondary tars (e.g., phenols, cresols and toluene) could be initially transformed into the tertiary tars (e.g., naphthalene) and adsorbed into the mesopores and macropores of char in accord with the result. For instance, light tars (e.g., naphthalene, indene) was adsorbed by RHC due to its high porosity property)[35]. It is concluded that the char-supported catalysts would be favor of the non-condensable tar conversion by intensive sorption, contributing to the increase of the residence time, and thereby improving catalytic efficiency. Therefore, the majority tars consisting of condensable and non-condensable tar were thermally cracked/reformed by *in-situ* catalysis, and thus transformed into the additional gaseous products. Figure S-3B showed the peak zone of C=O bonds (1600-1800 cm^{-1}) in RHCs, whose peak densities were weakened or disappeared after the pyrolysis. It indicated that, on one hand, the RH pyrolysis efficiency can be significantly improved by nickel impregnation or $NaBH_4$ modification; on the other hand, the above presented hydrolysis effect can indeed enhance the deoxygenation of C=O functional compounds in RH. For instance, the peak intensities of C=O in γ-lactones at ~1772 cm^{-1}, in δ-lactones at ~1733 cm^{-1}, were weakened possibly caused by lactones hydrolysis corresponding to the GC-MS results.

3.6. XRD Analysis of RHC Ni and Ni-B

RHs contain a variety of components such as lignin (20-30%), cellulose (55-65%) and silica (15-20%). As above, the lignin and cellulose can be transformed into the applicable energy products (e.g., syngas),

whilst the silica in RHs has a large potential for further research targeting more valuable applications (e.g., lithium battery anodes)[45]. The silica in RHs has developed unique porous nanostructures through years of natural evolution[46]. It can be observed that the pyrolytic RHC exhibits a broad silica (SiO_2) characteristic peak around $2\theta = 22.5^o$, representing the crystal structure of amorphous silica (Fig.4A). In addition, the high-purity of silica (~94.64% in RHA) resulting from the thermal treatment alone is substantially higher than those of the other silica resources, such as quartz, zeolites, which are prepared by similar procedures. In this research, the RHC produced from RH pyrolysis was further investigated as a carbon-based catalyst for tar conversion. Fig.4B shows the X-ray diffraction (XRD) patterns of the RHC Ni and RHC Ni-B. The characteristic peaks of amorphous silica (SiO_2) can be clearly observed as well. It suggests RHC, indeed, could be used as a stable catalyst support due to high-purity SiO_2. Table 4 lists the XRD characteristic peaks of the RHC Ni and RHC Ni-B. It is noteworthy that the main chemical states of nickel in the RHC Ni was in the forms of nickel oxides (e.g., bunsenite) and metallic nickel (Ni^0) corresponding to the reactions (1)-(3). Initially, the Ni^{2+} cations in aqueous solution were transformed into the relative stable form of $Ni(H_2O)_6^{2+}$ (i.e., octahedral water coordination complexes)[19], subsequently decomposed into NiO by thermochemical reactions. The partial metallic nickel (Ni^0) may be preliminary generated via *in-situ* deoxidation by reducing gases (e.g., CO, H_2) and carbon atoms during the pyrolysis process in the absence of oxygen (R23-R29) [18]. However, the characteristic peaks of NiO disappeared, whilst the chemical state of nickel was the synthesized Ni^0 in the RHC Ni-B. It is concluded that $NaBH_4$ modification can deoxidate the nickel oxide (i.e., NiO) into the metallic nickel (Ni^0), possibly enhancing the tar conversion efficiency by nickel catalytic reforming. Indeed, the active phase of Ni-based catalysts for hydrocarbon cracking (R28) and reforming reactions (e.g., R29), particularly methane (CH_4) catalytic reforming, is the metallic nickel (i.e., Ni^0) [47]. Besides, it has been reported that the XRD peak shifting and broaden may indicate the changes of crystal structures, for instance, enlargement or shrink of crystal cells, due to the interaction between crystals[48]. It can be found that the characteristic peaks of amorphous SiO_2 in the RHC slightly shifted to the left (lower angle) in both the RHC Ni and the RHC Ni-B; Likewise, the metallic nickel (Ni^0) characteristic peaks at 51.64^o and 76.23^o in the RHC Ni-B shifted to the left compared to the Ni^0 characteristic peaks at 51.67^o and 76.52^o, respectively, in RHC Ni, possibly indicating the enlargement of SiO_2 and Ni^0 crystal cells. Conversely, the Ni^0 strong characteristic peak at 44.45^o in the RHC Ni-B slightly shifted to the right (higher angle) compared to the corresponding Ni^0 characteristic peak at 44.43^o in the RHC Ni, indicating the shrinkage of the Ni^0 crystal cells.

$Ni_xO_yH_z + xC \rightarrow Ni_x + (2x\text{-}y)CO + (y\text{-}x)CO_2 + (z/2)H_2$ (R23)

$Ni_xO_yH_z + xC \rightarrow Ni_x^0 + xCO_{(ads)} + (y\text{-}x)OH_{(ads)} + (z\text{-}y+x)H_{(ads)}$ (R24)

$NiO + C \rightarrow Ni + CO$ (R25)

$NiO + CO \rightarrow Ni + CO_2$ (R26)

$NiO + H_2 \rightarrow Ni + H_2O$ (R27)

$C_xH_yO_z \rightarrow zCO + (y/2)H_2 + (x\text{-}nz)C$ (R28)

$C_xH_yO_z + H_2O \rightarrow xCO + (x+y/2\text{-}z)H_2$ (R29)

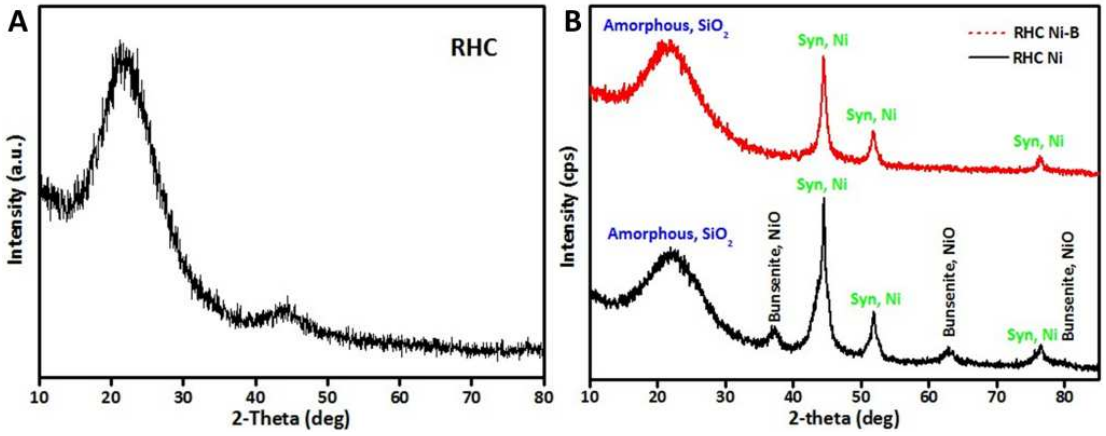

Figure 4. XRD curves of (A) raw RHC, (B) RHC Ni and Ni-B

Table 4. XRD Characteristic Peak Lists of RHC Ni and RHC Ni-B

No.	2-theta (deg)	d (ang.)	Height (cps)	FWHM (deg)	Int. I (cps deg)	Size (ang.)	Phase name
Peak list of RHC Ni							
1	22.37(13)	3.97(2)	149(12)	8.52(11)	1351(30)	9.93(12)	Amorphous SiO_2
2	37.21(18)	2.414(11)	30(5)	1.59(16)	54(12)	55(5)	Nickel Oxide(1,0,1), Bunsenite(1,1,1)
3	43.63(17)	2.073(8)	124(11)	2.45(10)	353(38)	36.5(15)	Nickel Oxide(0,1,2), Bunsenite(2,0,0)
4	44.43(2)	2.0373(9)	288(17)	0.46(6)	259(37)	195(24)	Nickel, syn(1,1,1)
5	51.67(3)	1.7677(9)	96(10)	1.06(4)	141(6)	87(3)	Nickel, syn(2,0,0)
6	62.76(14)	1.479(3)	36(6)	2.2(2)	159(7)	44(5)	Nickel Oxide(1,1,0), Bunsenite(2,2,0)
7	76.52(9)	1.2439(12)	38(6)	1.70(12)	92(5)	62(4)	Nickel, syn(2,2,0), Nickel Oxide(0,2,1), Bunsenite(3,1,1)
Peak list of RHC Ni-B							
1	21.44(10)	4.140(19)	191(14)	8.83(9)	1898(23)	9.56(10)	Amorphous SiO_2
2	44.45(2)	2.0366(11)	241(16)	0.75(4)	330(6)	119(6)	Nickel, syn(1,1,1)
3	51.64(2)	1.7685(7)	65(8)	0.97(6)	80(4)	95(6)	Nickel, syn(2,0,0)
4	76.23(14)	1.2480(19)	23(5)	0.84(11)	21(3)	126(16)	Nickel, syn(2,2,0)

3.7. TEM Analysis of RHC Ni-B

It has been demonstrated that the metallic nickel (Ni^0) nanoparticles, which were dispersed uniformly in the carbon matrix, were undetected in the wood char obtained at pyrolysis temperatures from 500 to 700 ^oC. However, the very wide dispersion of the monocrystalline metallic nickel (Ni^0) particles with the particle size of 2-4 nm could form at the pyrolysis temperatures from 400 to 500 ^oC and their nanometric size confirmed the high dispersion of the metal precursor in the wood obtained after the impregnation step [19]. Figure S-4 shows the TEM images of the RHC Ni-B. It can be observed remarkably that the most of agglutinated metallic nickel (Ni^0) particles with the particle size of 10-20 nm dispersed uniformly, most likely due to the coagulation with the nanosized amorphous silica. The smaller-sized Ni^0 nanoparticles can also be obtained probably by using an impregnation method favoring high dispersion of Ni^{2+} species on the carbon matrix of RHC. Furthermore, other elements distributed around the Ni nanoparticle, such as Mg, Si, K, Ca, can be detected as similar as the chemical constitutes in the ash. In addition, the TEM-EDS semi-quantitative result of the RHC Ni-B was also shown in Fig.5. It can be found that Ni, Si and C were the main element constitutes existed in the RHC Ni-B, while boron (B) and sodium (Na) were not detected. The reason might be that their concentrations were much lower than C and Ni in the analyzed central point of particle. It can be concluded that most of nickel nanoparticles existed in the form of polymolecularity metallic nickel (Ni^0) or conglutinated with the crystalline silica, and thus other nickel nanoparticles might be transformed into Ni_xB or dispersed independently in the carbon matrix of RHC.

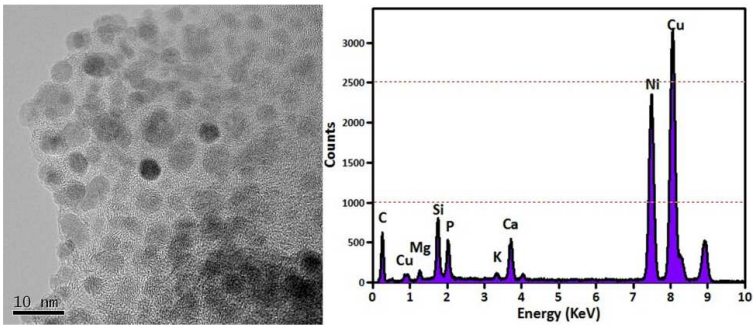

Figure 5. TEM images and EDS analysis of RHC Ni-B at 200 kV

3.8. Catalytic Performances of RHC Ni and Ni-B

The biomass or biochar could be employed for heavy metal (e.g., Ni) wastewater treatment. Consequently,

454 it is encouraged to use the solid pyrolytic biochar (i.e, RHC, RHC Ni, and RHC Ni-B) as a carbon-based
455 catalyst for tar conversion. In addition, the produced biochar could be further activated or directly catalytic
456 gasified into the applicable syngas. Fig.6 shows the tar yields from RH co-pyrolysis with RHC catalysts at
457 750 ^{o}C. It can be found that RHC itself showed catalytic activity for tar conversion due to the presence of
458 minerals. Klinghoffer et al. [49] thought the minerals and/or metals such as iron in the polar wood char
459 most likely play a role in the hydrocarbons catalytic cracking reactions. After being used for catalytic
460 reactions, carbon deposition would occur on the iron clusters and the pores of the char surface influencing
461 the catalytic activity. Char from pyrolysis/gasification provides a high surface area support for the ash,
462 which is already impregnated in the char, thereby producing a supported metal catalyst. Thus, it has
463 proved the char catalysts continuously generated on-site in the pyrolysis/gasification process, have a
464 potential to replace expensive tar decomposition catalysts. If raw RH was mixed with the RHC Ni and
465 RHC Ni-B, the condensable tar could be significantly removed by 96.5% and 92.6%, respectively.
466 Nevertheless, the catalytic performance shows a slight decrease compared with the directly pyrolysis of
467 the RH Ni and Ni-B, implying that the addition of $NaBH_4$ can enhance the tar conversion and upgrade the
468 vapor during RH Ni-B pyrolysis, but the solid residues of RHC Ni-B showed a slight inferior of catalytic
469 performance, especially in terms of tar conversion. One main reason may also be ascribed to the mass
470 ratio decrease of nickel particles. It is worth pointing out that the RHC Ni exhibited a comparable tar
471 conversion efficiency compared to the directly pyrolysis of RH Ni. Based on the above FTIR analysis, to
472 some extent, a higher tar conversion efficiency of the RHC Ni may also be attributed to its better tar
473 adsorbability. Lately, some researchers thought that B_2O_3 addition can result in the larger metal Ni
474 particles and strong Lewis acidic boron sites, which are responsible for the fast carbon accumulation on
475 the catalyst and the deactivation during dry reforming[23]. In this study, the characteristic peak intensity of
476 amorphous silica decreasing followed by the enlarged SiO_2 crystal cells, may be attributed to the
477 coagulation of NiO and SiO_2. Meanwhile, Ni_xB were undetected in the RHC Ni-B by XRD and EDS point
478 analysis, accompanied by the intensity decrease of metallic nickel (Ni^0) particles in the XRD spectra. It
479 can infer that the surfaces of nickel particles, especially for NiO, were easily accumulated and wrapped by
480 carbon deposition. Furthermore, the service life, deactivation mechanisms and catalytic kinetics of the
481 RHC Ni catalysts for tar reforming would be studied in the gasifier (*in situ*) [50] or in the reformer (*ex situ*)
482 in details. Besides, it was reported that the nano-NiO/Al_2O_3 catalyst showed the excellent activity of tar
483 reforming in biomass gasification [51]. Scheme 4 presents the mechanisms of the RHC Ni-B generation,

deactivation and recycle. A key point of the proposed strategy is the catalyst recovery and reuse. Based on the nickel balance calculation, it can indicate that a mean nickel recovery is about 100% in the biochar, since metal nickel is not lost by volatilization [18]. The research efforts are still required to study the reaction and deactivation mechanisms involved in such a catalytic process under various heating rates, atmosphere and pressure conditions encountered in pyrolytic gasification processes to identify the optimal process condition. Consequently, the deactivated RHC Ni with the merit of low-cost would be thermally activated or directly catalytic gasified into the applicable syngas, accompanied by the production of the silica-based nickel (i.e., NiO/SiO_2) nanoparticles in the ash. It is noteworthy that the proposed catalytic pyrolysis technology should be seriously considered in the development of biomass pyrolytic gasification and high value-added materials production. In the view of bioenergy, the biomass pretreatment prior to fast pyrolysis indeed has significantly influenced on the yield and product distribution [52,53]. As for the synthesis of material, more environmental-friendly metal precursors could be considered, such as iron oxide nanoparticle catalysts embedded in the carbon matrix [54,55].

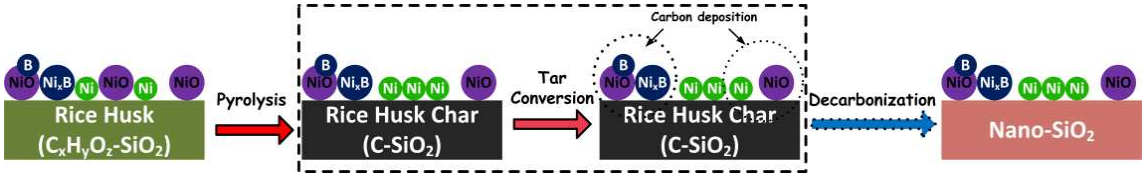

Scheme 4. Possible mechanisms of RHC Ni-B catalysts generation, deactivation and recovery

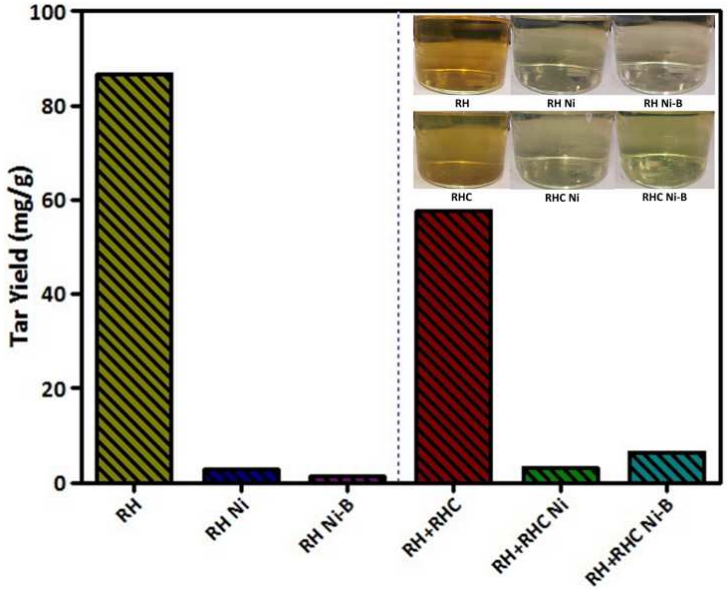

Figure 6. Tar yields from RH co-pyrolysis with RHC Ni and Ni-B (mass ratio: 1) at 750 °C

4. CONCLUSIONS

An integrated approach of *in-situ* tar and syngas conversion technology has been proposed for biomass pyrolysis/gasification by the pretreatment of nickel impregnation combined with sodium borohydride ($NaBH_4$) modification, which is also a potential method for nickel nanoparticles *in situ* generated in RHC. The ultra-low tar yield can be achieved by pyrolysis of RH Ni and RH Ni-B, especially in terms of high removal efficiencies of 96.9% and 98.6%, respectively, compared to the raw RH pyrolysis at 750 ^{o}C. On one hand, the removed tar was converted into the extra gases by thermochemical reactions (i.e., cracking, reforming) with Ni catalysis effect; on the other hand, the Ni-based catalyst could enhance the pyrolysis efficiency and restrain at source the formation of condensable tar due to polymerization. In addition, the condensed tar compounds existed mainly in the forms of mononuclear aromatics (e.g., benzene derivates, furan derivates) and oxygenated aromatic compounds (e.g., phenolic derivatives, alcohol derivatives, acid derivatives). However, only trace amounts of the light single-ring tar compounds (e.g., benzene, toluene) and polycyclic aromatic hydrocarbons were detected in the tar. It is noteworthy that the condensable tar could be catalytically transformed into the non-condensable tar or small molecule gases resulting in the heating value increase of gaseous products to benefit of the power generation systems, corresponding to the LHV of syngas increased from 10.25 to 11.32 MJ/m^3. In this research, the metallic nickel species coexisted with some nickel oxides caused by the partial *in-situ* reduction of NiO by the carbon atoms or reducing gas (e.g., H_2, CO). Also, the formed polymolecularity Ni^0 might be attributed to the disproportionated reaction and strong reducing property of $NaBH_4$, which reduced NiO into Ni^0 improving the catalytic activity. Compared with the conventional methods for catalysts preparation by hydrogenation reduction at high temperature and pressure, this approach is much easy and energy-saving. Interestingly, the pyrolytic residues of RHC Ni and RHC Ni-B also showed the good catalytic performances on tar conversion. The condensable tar derived from RH could be significantly removed by 96.5% and 92.6%, respectively, by co-pyrolysis with the RHC Ni and/or RHC Ni-B. In the future work, the catalytic activity and kinetics, service life (i.e., use longevity) and deactivation mechanisms of these catalysts employed for tar *ex situ* conversion would be studied and conducted in the reformer.

ACKNOWLEDGEMENTS

The authors would like to appreciate the Chinese Scholarship Council (CSC) for the financial support under Grant No.201206230168. We also thank Dr. Hongbo Zhang from Shanghai Jiaotong University (SJTU) for GC-MS measurement. In addition, we are grateful to editors and reviewers for their valuable comments.

SUPPORTING INFORMATION

The supplementary materials are as follows. Figure S-1 presents the condensable tar yields of RHs pyrolysis at 750 ^{o}C; Figure S-2 shows the GC-MS spectra of the collected tar samples; Figure S-3 shows the FTIR spectra of RHs before and after pyrolysis; Figure S-4 shows the FE-TEM images of the RHC Ni; Table S-1 shows the ultimate and proximate analysis of RHs;

REFERENCES

[1] H.B. Goyal, D. Seal, R.C. Saxena, Bio-fuels from thermochemical conversion of renewable resources: a review. *Renew. Sust. Energy Rev.* 2008, 12, 504-517.

[2] I. Demiral, S. Sensoz, The effects of different catalysts on the pyrolysis of industrial wastes. *Bioresour. Technol.* 2008, 99, 8002-8007.

[3] G.W. Huber, S. Iborra, A. Corma, Synthesis of transportation fuels from biomass: chemistry, catalysts, and engineering. *Chem. Rev.* 2006, 106, 4044-4098.

[4] M. Stocker, Biofuels and biomass-to-liquid fuels in the biorefinery: catalytic conversion of lignocellulosic biomass using porous materials, *Angew. Chem. Int. Edit.* 2008, 47, 9200-9211.

[5] L. Zhou, H. Yang, H. Wu, M. Wang, D. Cheng, Catalytic pyrolysis of rice husk by mixing with zinc oxide: Characterization of bio-oil and its rheological behavior. *Fuel Process. Technol.* 2013, 106, 385-391.

[6] L. Devi, K.J. Ptasinski, F.J.J.G. Janssen, A review of the primary measures for tar elimination in biomass gasification processes. *Biomass Bioenerg.* 2003, 24, 125-140.

[7] Y. Shen, K. Yoshikawa, Recent Progresses in Catalytic Tar Elimination during Biomass Gasification or Pyrolysis – A Review. *Renew. Sust. Energy Rev.* 2013, 21, 371-392.

[8] C. Wu, P.T. Williams, Nickel-based catalysts for tar reduction in biomass gasification. *Biofuels* 2011, 2(4), 451-464.

[9] J.N. Kuhn, Z.K. Zhao, L.G. Felix, R.B. Slimane, C.W. Choi, U.S. Ozkan, Olivine catalysts for methane- and tar-steam reforming. *Appl. Catal. B: Environ.* 2008, 81, 14-26.

[10] R.Q. Zhang, Y.C. Wang, R.C. Brown, Steam reforming of tar compounds over Ni/olivine catalysts doped with CeO_2. *Energy Convers. Manage* 2007, 48, 68-77.

[11] P.T. Williams, P.A. Horne, The influence of catalyst type on the composition of upgrade biomass

pyrolysis oil. *J. Anal. Appl. Pyrol.* 1995, 31, 39-61.

[12] A. Aho, N. Kumar, K. Eranen, T. Salmi, M. Hupa, D.Y. Murzin, Catalytic pyrolysis of woody biomass in a fluidized bed reactor: influence of the zeolite structure. *Fuel* 2008, 87, 2493-2501.

[13] C. Couhert, J.M. Commandre, S. Salvador, Is it possible to predict gas yields of any biomass after rapid pyrolysis at high temperature from its composition in cellulose, hemicellulose and lignin? *Fuel* 2009, 88, 408-417.

[14] F. Ates, A.E. Putun, E. Putun, Pyrolysis of two different biomass samples in a fixed-bed reactor combined with two different catalysts. *Fuel* 2006, 85, 1851-1859.

[15] K. Bru, J. Blin, A. Julbe, G. Volle, Pyrolysis of metal impregnated biomass: An innovative catalytic way to produce gas fuel. *J. Anal. Appl. Pyrol.* 2007, 78, 291-300.

[16] Q. Fu, D.S. Argyropoulos, D.C. Tilotta, L.A. Lucia, Understanding the pyrolysis of CCA-treated wood. Part I. Effect of metal ions. *J. Anal. Appl. Pyrol.* 2008, 81, 60-64.

[17] F.X. Collard, J. Blin, A. Bensakhria, J. Valette, Influence of impregnated metal on the pyrolysis conversion of biomass constitutes. *J. Anal. Appl. Pyrol.* 2012, 95, 213-226.

[18] Y. Richardson, J. Blin, G. Volle, J. Motuzas, A. Julbe, In Situ Generation of Ni Metal Nanoparticles as Catalyst for H_2-Rich Syngas Production from Biomass Gasification. *Appl. Catal. A: Gen.* 2010, 382, 220-230.

[19] Y. Richardson, J. Motuzas, A. Julbe, G. Volle, and J. Blin, Catalytic Investigation of in Situ Generated Ni Metal Nanoparticles for Tar Conversion during Biomass Pyrolysis. *J. Phys. Chem. C* 2013, 117, 23812-23831.

[20] L. Vilaescusa, N. Fiol, M. Martinez, N. Miralles, J. Poch, J. Serarols, Removal of copper and nickel ions from aqueous solutions by grape stalks wastes. *Water Research* 2004, 38, 992-1002.

[21] Q. Lu, C.Q. Dong, X.M. Zhang, H.Y. Tian, Y.P. Yang, X.F. Zhu, Selective fast pyrolysis of biomass impregnated with $ZnCl_2$ to produce furfural: analytical Py-GC/MS study. *J. Anal. Appl. Pyrol.* 2011, 90, 204-212.

[22] J. Wang, M. Zhang, M. Chen, F. Min, S. Zhang, Z. Ren, Y. Yan, Catalytic effects of six inorganic compounds on pyrolysis of three kinds of biomass. *Thermochim. Acta* 2006, 444, 110-114.

[23] J. Ni, L. Chen, J. Lin, S. Kawi, Carbon deposition on borated alumina supported nano-sized Ni catalysts for dry reforming of CH_4. *Nano Energy* 2012, 1, 674-686.

[24] T. Chen, H. Liu, P. Shi, D. Chen, L. Song, H. He. R.L. Frost, CO_2 reforming of toluene as model compound of biomass tar on Ni/Palygorskite. *Fuel* 2013, 107, 699-705.

[25] M.C.J Bradford, M.A. Vannice, CO_2 Reforming of CH_4. *Catal. Rev. Sci. Eng.* 1999, 41, 1-42.

[26] Y.H. Hu, E. Ruckenstein, Catalytic Conversion of Methane to Synthesis Gas by Partial Oxidation and CO_2 Reforming. *Adv. Catal.* 2004, 48, 297-345.

[27] A. Fouskas, M. Kollia, A. Kambolis, Ch. Papadopoulou, H. Matralis, Boron-modified Ni/Al_2O_3 catalysts for reduced carbon deposition during dry reforming of methane. *Appl. Catal. A: Gen.* 2013, in press.

[28] M. Kong, Q. Yang, J. Fei, X. Zheng, Experimental study of Ni/MgO catalyst in carbon dioxide reforming of toluene, a model compound of tar from biomass gasification. *Int. J. Hydrogen Energy* 2012, 37, 13355-13364.

[29] C. Courson, E. Makaga, C. Petit, A. Kiennemann, Development of Ni catalysts for gas production from biomass gasification. Reactivity in steam- and dry-reforming. *Catal. Today* 2000, 63, 427-437.

[30] J. Xu, M. Saeys, First Principles Study of the Effect of Carbon and Boron on the Activity of a Ni Catalyst. *J. Phys. Chem. C* 2009, 113, 4099-4106.

612 [31] J. Xu, L. Chen, K.F. Tana, A. Borgna, M. Saeys, Effect of boron on the stability of Ni catalysts during
613 steam methane reforming. *J. Catal.* 2009, 261, 158-165.

614 [32] J.C.S. Wu, H.C. Chou, Bimetallic Rh-Ni/BN catalyst for methane reforming with CO_2. *Chem. Eng. J*
615 2009, 148, 539-545.

616 [33] G. Garbarino, E. Finocchio, A. Lagazzo, I. Valsamakis, P. Riani, V.S. Escribano, G. Busca, Steam
617 reforming of ethanol-phenol mixture on Ni/Al_2O_3: Effect of magnesium and boron on catalytic activity in
618 the presence and absence of sulphur. *Appl Catal B: Environ.* 2014, 147, 813-826.

619 [34] W.J. Wang, M.H. Qiao, H.X. Li, W.L. Dai, J.F. Deng, Study on the deactivation of amorphous
620 NiB/SiO_2 catalyst during the selective hydrogenation of cyclopentadiene to cyclopentene. *Appl. Catal. A:*
621 *Gen.* 1998, 168, 151-157.

622 [35] A. Paethanom, S. Nakahara, M. Kobayashi, P. Prawisudha, K. Yoshikawa, Performance of tar
623 removal by absorption and adsorption for biomass gasification. *Fuel Process. Technol.* 2012, 104,
624 144-154.

625 [36] W. Wang, J.C. Martin, N. Zhang, C. Ma, A. Han, L. Sun, Harvesting silica nanoparticles from rice
626 husks. *J. Nanoparticle Res.* 2011, 13, 6981-6990.

627 [37] H. Yang, R. Yan, H. Chen, D.H. Lee, C. Zheng, Characteristics of hemicellulose, cellulose and lignin
628 pyrolysis. *Fuel* 2007, 86, 1781-1788.

629 [38] A. Meng, H. Zhou, L. Qin, Y. Zhang, Q. Li, Quantitative and kinetic TG-FTIR investigation on three
630 kinds of biomass pyrolysis. *J. Anal. Appl. Pyrol.* 2013, 104, 28-37.

631 [39] Y. Shen, T. Sun, J. Jia, Novel desulfurization method of sodium borohydride reduction for coal water
632 slurry. *Energy Fuels* 2011, 25, 2963-2967.

633 [40] M. Liu, H. Wang, J. Han, Y. Niu, Enhanced hydrogenolysis conversion of cellulose to C2-C3 polyols
634 via alkaline pretreatment. *Carbohyd. Polym.* 2012, 89, 607-612.

635 [41] Y. Copur, A. Tozluoglu, O. Ozyurek, Sodium borohydride ($NaBH_4$) pretreatment for efficient
636 enzymatic saccharification of wheat straw. *Bioresour. Technol.* 2012, 107, 258-266.

637 [42] M.S Fan, A.Z. Abdullah, S. Bhatia, Catalytic technology for carbon dioxide reforming of methane to
638 synthesis gas. *ChemCatChem* 2009, 1, 192-208.

639 [43] R. Lu, G.P. Sheng, Y.Y. Hu, P. Zheng, H. Jiang, Y. Tang, H.Q. Yu, Fractional characterization of a
640 bio-oil derived from rice husk. *Biomass Bioenerg.* 2011, 671-678.

641 [44] R.M. Baldwin, K.A. Magrini-Bair, M.R. Nimlos, P. Pepiot, B.S. Donohoe, J.E. Hensley, S.D. Phillips,
642 Current research on thermochemical conversion of biomass at the National Renewable Energy Laboratory.
643 *Appl. Catal. B: Environ.* 2012, 115-116, 320-329.

644 [45] N. Liu, K. Huo, M.T. McDowell, J. Zhao, Y. Cui, Rice husks as a sustainable source of
645 nanostructured silicon for high performance Li-ion battery anodes. *Sci. Rep.* 2013, 3, 1919.

646 [46] D.S. Jung, M-H. Ryou, Y.J. Sung, S.B. Park, and J.W. Choi, Recycling rice husks for high-capacity
647 lithium battery anodes. *Proc. Natl. Acad. Sci. U.S.A.* 2013, 110, 12229-12234.

648 [47] W. Torres, S.S. Pansare, J.G. Goodwin, Hot gas removal of tars, ammonia, and hydrogen sulfide from
649 biomass gasification gas. *Catal. Rev. Sci. Eng.* 2007, 49, 407-456.

650 [48] N. Yuzer, Z. Cinar, F. Akoz, H. Biricik, Y.Y. Gurkan, N. Kabay, A.B. Kizilkanat, Influence of raw rice
651 husk addition on structure and properties of concrete. *Constr. Build. Mater.* 2013, 44, 54-62.

652 [49] N.B. Klinghoffer, M.J. Castaldi, and A. Nzihou, Catalyst Properties and Catalytic Performance of
653 Char from Biomass Gasification. *Ind. Eng. Chem. Res.* 2012, 51, 13113-13122.

654 [50] Y. Shen, K. Yoshikawa, Tar conversion and vapor upgrading via in-situ catalysis using silica-based

655 nickel nanoparticles embedded in rice husk char for biomass pyrolysis/gasification. *Ind. Eng. Chem. Res.*
656 2014, 53, 10929-10942.

657 [51] J. Li, R. Yan, B. Xiao, D.T. Liang, L. Du, Development of Nano-NiO/Al_2O_3 Catalyst to be Used for
658 Tar Removal in Biomass Gasification. *Environ. Sci. Technol.* 2008, 42, 6224-6229.

659 [52] D. Carpenter, T.L. Westover, S. Czernik, W. Jablonski, Biomass feedstocks for renewable fuel
660 production: a review of the impacts of feedstock and pretreatment on the yield and product distribution of
661 fast pyrolysis bio-oils and vapors. *Green Chem*. 2014, 16, 384-406.

662 [53] S. Du, J.A. Valla, G.M. Bollas, Characteristics and origin of char and coke from fast and slow,
663 catalytic and thermal pyrolysis of biomass and relevant model compounds. *Green Chem.* 2013, 15,
664 3214-3229.

665 [54] Q. Yan, C. Wan, J. Liu, J. Gao, F. Yu, J. Zhang, Z. Cai, Iron nanoparticles in situ encapsulated in
666 biochar-based carbon as an effective catalyst for the conversion of biomass-derived syngas to liquid
667 hydrocarbons. *Green Chem*. 2013, 15, 1631-1640.

668 [55] W. Hao, E. Björkman, Y. Yun, M. Lilliestråle, N. Hedin, Iron oxide nanoparticles embedded in
669 activated carbons prepared from hydrothermally treated waste biomass. *ChemsusChem* 2014, 7, 875-882.

Graphical Abstract

The upgraded tar-free syngas could be produced from catalytic pyrolysis of biomass impregnated with nickel cations and modified by $NaBH_4$, accompanied by in situ generation of the recyclable silica-based metallic nickel (Ni^0) nanoparticles embedded in rice husk char.